NUKLEONIKA 2012;57(4):435–441

ORIGINAL PAPER

Depletion analysis of the HELIOS experiment using the MCB code

**Mikołaj Oettingen,
Elio D'Agata,
Christoph Döderlein,
Kamil Tuček,
Jerzy Cetnar**

Abstract. The focus of our studies is to present an advanced depletion analysis of the HELIOS experiment by means of the Monte Carlo continuous energy burn-up code (MCB). The MCB was used mainly to calculate nuclide density evolution in nuclear reactor cores. We present the capability of the MCB to investigate the depletion of nuclear fuel samples irradiated in the HELIOS experiment. In our studies we traced the behaviour of the main fissile isotopes, ^{242m}Am and ^{239}Pu, respectively. We also perform a sensitivity analysis to the choice of JEF2.2 and JEFF3.1 cross section libraries in terms of the released fission power and the evolution of actinide inventories. The amount of He produced at the end of irradiation, as well as Am and Pu depletion, were also considered.

Key words: depletion • HELIOS • Monte Carlo continuous energy burn-up code (MCB) • minor actinides

M. Oettingen✉
AGH University of Science and Technology,
al. A. Mickiewicza 30, 30-059 Krakow, Poland
and European Commission, Joint Research Centre,
Institute for Energy,
P. O. Box 2, 1755 ZG Petten, The Netherlands,
Tel.: +48 12 617 4420, Fax: +48 12 634 0010,
E-mail: moettin@agh.edu.pl

E. D'Agata, C. Döderlein, K. Tuček
European Commission, Joint Research Centre,
Institute for Energy,
P. O. Box 2, 1755 ZG Petten, The Netherlands

J. Cetnar
AGH University of Science and Technology,
al. A. Mickiewicza 30, 30-059 Krakow, Poland

Received: 24 November 2011
Accepted: 25 January 2012

Introduction

The considerable reduction of mass and radiotoxicity of the spent nuclear fuel inventory may be achieved by incinerating minor actinides (MAs) in the fast spectrum reactors. The innovative nuclear fuel for such reactors consists of two major components, fissile material and the neutron-transparent matrix in which this material is permanently embedded. Both fuel and matrix must fulfil many mechanical, neutronic, chemical and other requirements under irradiation conditions. The influence of irradiation conditions on the fuel and matrix in the nuclear reactor core can only be reliably estimated in the irradiation experiments. Moreover, particular attention should be paid to further experimental and analytical post irradiation examination (PIE).

An irradiation experiment, called HELIOS [6], was designed as a part of the EUROTRANS project during the 6th Framework Programme of the European Union. The main goal of EUROTRANS was the generic conceptual design of a modular European Facility for Industrial Transmutations (EFIT) and the advanced design of an experimental facility demonstrating the technical feasibility of transmutation in accelerator-driven systems (ADS).

The reason for announcing the HELIOS experiment were the results obtained in the previous irradiations of inert matrix fuels in the Petten high flux reactor (HFR), performed in the collaboration on the Experimental Feasibility of Targets for Transmutation (EFTTRA) [15]. The most recent irradiated samples (EFTTRA-4

and EFTTRA-4bis) contained a 10–12 wt% ^{241}Am fraction in different inert matrices [14]. The PIE revealed high diametrical swelling caused by production of fission gases and He from α decay of Cm isotopes, especially ^{242}Cm. The investigation of this effect was the major goal of a new dedicated experiment – HELIOS.

The main purpose of the experiment was to gain knowledge about the in-pile behaviour of uranium-free fuels containing americium, as well as to investigate the influence of microstructure and temperature on fuel swelling and He release. Two different approaches were applied to ensure He release from the initial stage of irradiation: creation of open porosity with release paths; and introduction of Pu in order to increase sample power and, as a result, irradiation temperature.

In our studies we present major findings obtained from depletion analysis of the HELIOS experiment using the MCB code equipped with JEFF3.1 [13] and JEF2.2 [1] cross section libraries. We focus our attention on the time-lines of the main actinide nuclides and released fission power. In section 'The HELIOS experiment' we explain the layout of the experiment. Section 'Method' describes the numerical method while section 'Calculations tools' focuses on the description of the MCB code. The results are outlined in section 'Results'. Finally, section 'Conclusions' summarizes the analysis performed and points to the future direction of the elaboration of the HELIOS experiment.

The HELIOS experiment

In total, five different fuel samples were irradiated in the HFR at the in-core position G7 from April 2009 to February 2010, which gives about 240 equivalent full power days. The long-lived ^{241}Am contributes significantly to the radiotoxic inventory of spent nuclear fuel. As a result, all fuel samples consisted of ^{241}Am dispersed in different inert matrices. The Pu was only present in samples 3 and 5. Sample 1 contained ceramic-ceramic (CerCer) type fuel pellets made of the $Am_2Zr_2O_7$ particles heterogeneously mixed with the MgO inert matrix material. The americium in samples 2 and 3 was incorporated in a crystal lattice of the inert matrix forming a solid solution with Zr and Y. The fuel samples 4 and 5 were Mo based ceramic-metallic (CerMet) composite pellets with a spherical particle diameter of about 100 μm.

The experiment consists of two specimen holders (HELIOS-1 and HELIOS-2), loaded into two out of four irradiation channels of the reloadable QUATRO 129 rig. The remaining two channels were filled with Al dummies. The schematic view of the experiment is shown in Fig. 1. To ensure uniform distribution of neutron flux, the orientation of the QUATRO 129 rig was changed by 180° at every reactor cycle. The temperature of the experiment was adjusted by two independent systems. First, the specimen holders embedded in irradiation channels were fitted in a vertical displacement unit (VDU), which allows axial movement of both specimen holders together and, as a result, usage of the effect of flux buckling. Second, the gas gap between the QUATRO 129 channel and sample holder may be filled with a mix of He, Ne and N. The thermal conductivities

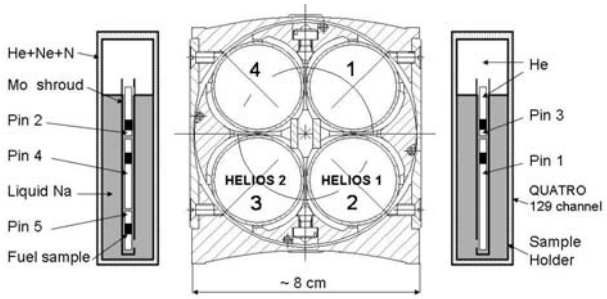

Fig. 1. Schematic view of QUATRO 129 with four irradiation channels and radial cross cuts of the HELIOS-1 and HELIOS-2 specimen holders.

of the three gases mentioned are different, which can lead to changes in the temperature of the samples. At the beginning of irradiation, the gas gap was filled with pure He, and the VDU was set to the lowest possible position. The pins with fuel samples inside were placed in a Mo shroud inside a sodium bath. The upper part of the design, above the sodium level, was filled with He. The Mo shroud acted as a carrier for the fluence detector sets, thermocouples and other instrumentation. The fuel pins contained fuel samples in the He atmosphere.

Method

The numerical analysis of the HELIOS experiment consists of two main steps. In the first step, the source strengths and neutron spectra impinging the fuel samples are calculated in what are known as MOTIF calculations [7]. The estimated source parameters were then used in the short-time depletion runs using the MCB code in mode with an external neutron source. The reason for introducing a two-step strategy lies in the Monte Carlo (MC) uncertainty estimation. First, the numerical modelling of only the essential part of the HFR core gives lower uncertainties and shorter computation time, together with sufficient reconstruction of the neutron environment around the fuel samples. Second, the numerical model for the external source calculations is characterized by very simple geometry, which also ensures low statistical uncertainities and short calculation times in the fuel depletion runs. This, in turn, makes it possible to investigate many aspects of the evolution of isotope density in a series of individual calculations with different initial parameters, such as cross section libraries, neutron spectra, source strengths, etc.

The MOTIF calculations correspond to the general method of estimating the irradiation environment in the HFR core and were performed using the MCNP code [2]. The numerical model includes only reactor components, which could have a significant influence on the experiments. Figure 2 presents the MOTIF configuration used to calculate the source parameters for the depletion analysis of the HELIOS samples. It takes into account vertical control rod (CR) movement at the position F6; 180° rotation and vertical movement of the experiment at the position G7; interpolation of fuel composition at the positions F7, G6, G8 and H7. The neutron transparent surveillance vessel and aluminium elements at the positions F8, H6 and

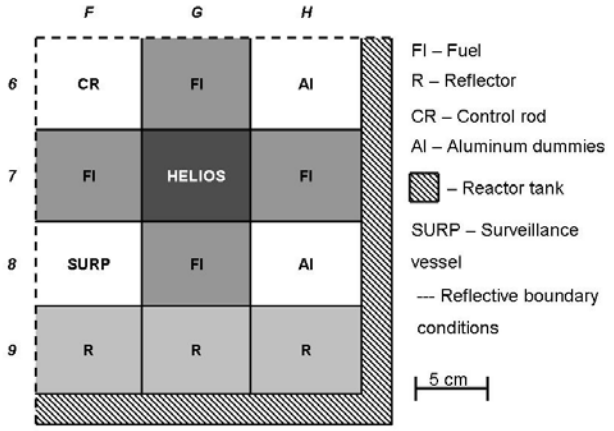

Fig. 2. MOTIF geometry.

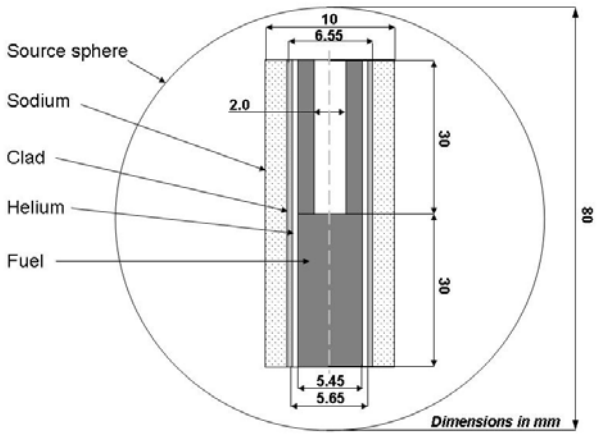

Fig. 3. Geometry of samples 2 and 3 applied in MCB source calculations.

H8 respectively, have a small influence on neutron spectrum, so we do not model any movement of these elements during irradiation. All parameters mentioned are reconstructed with reference to the HELIOS post cycle reports provided by the Nuclear Research and Consultancy Group, which is responsible for the operation of the HFR. The parameters are constant during the individual irradiation cycle, but change from cycle to cycle. The in-pile presence of neutron-absorbing material of the fuel samples may significantly interfere with the neutron spectrum and source strengths. Thus, the fuel samples in the MOTIF calculations were filled with neutron-transparent Al dummies, which minimize the impact on neutron flux. The neutron spectrum was scored on the cylindrical surface around the fuel samples and then placed on the source sphere in the MCB depletion calculations.

Figure 3 displays the geometry of the numerical model designed for the MCB source calculations. The fuel in samples 2 and 3 is divided into two subsections, which correspond to the volumes with the thermocouple (TC) hole and those without it. Samples 1, 4 and 5 are modelled in their entirety, without any subdivisions. In order to simplify the geometrical model, we do not simulate neutron-transparent TC, because its influence on the irradiation environment is negligible. Instead, we fill the TC hole with pure He. The initial isotopic composition of all five samples and their material and geometrical properties are set out in Table 1. The neutron spectrum sampled from the probability distribution for 172 XMAS [9] energy groups structure from the MOTIF runs was put on the source surface. The source strengths S_i for 9 irradiation cycles were estimated by means of the total neutron flux impinging on the samples ϕ_i, total MOTIF power P_i and total normalization factor F_{tot}, 3.41E+18, for nominal core power P_{nom}, 45 MW, using Eq. (1). The source strengths obtained for both samples and reactor cycles are quantified in Table 2.

$$S_i = \frac{\varphi_i \cdot P_i \cdot F_{\text{tot}}}{P_{\text{nom}}} \quad (i = 1,\ldots,9) \tag{1}$$

Table 1. Fuel parameters

Sample no.	Composition	Density (g/cm^3)		TD[a] measured (%)	Final density based on TD (g/cm^3)	Mass (g)	Volume (cm^3)
		Pu	^{241}Am				
S1	$MgO + Am_2Zr_2O_7$		0.66	91.50	3.96	5.54	1.40
S2	$(Am,Zr,Y)O_2$		0.70	92.60	5.91	7.71	1.31
S3	$(Pu,Am,Zr,Y)O_2$	0.41	0.74	89.70	5.95	7.77	1.31
S4	$(Am,Zr,Y)O_2 + Mo$		0.69	94.10	8.84	12.38	1.40
S5	$(Pu,Am)O_2 + Mo$	1.24	0.30	94.00	9.99	13.98	1.40

[a] TD – theoretical density.

Table 2. Source strengths for all five samples (S1 to S5) and nine irradiation cycles

Cycle	Duration (days)	S1	S2	S3	S4	S5
1	30.76	4.98E+14	3.63E+14	3.97E+14	4.45E+14	2.97E+14
2	24.69	3.93E+14	3.53E+14	3.20E+14	4.38E+14	2.86E+14
3	17.59	4.99E+14	3.47E+14	3.88E+14	4.39E+14	2.94E+14
4	22.08	3.89E+14	3.22E+14	2.96E+14	4.31E+14	3.03E+14
5	33.43	4.67E+14	2.67E+14	2.82E+14	4.18E+14	3.55E+14
6	24.75	3.62E+14	2.60E+14	2.42E+14	4.00E+14	3.50E+14
7	31.41	4.63E+14	3.00E+14	3.28E+14	4.12E+14	2.93E+14
8	24.34	4.06E+14	3.25E+14	2.98E+14	4.50E+14	3.45E+14
9	31.65	4.95E+14	3.48E+14	3.84E+14	4.39E+14	2.95E+14

Calculation tools

The MCB code

The MCB is a general-purpose tool for depletion analysis in transmutation and decay systems [4]. The Bateman equation, (Eq. (2)), governing such systems is solved using the linear chain method [3]. This means that the nonlinear transmutation and decay system is broken down into a set of linear chains and the solution is simply the superposition of individual chain solutions. Equation (2) presents the Bateman equation in the general matrix form, where $\vec{N}$ stands for the vector containing time dependent isotope densities, $\vec{N}_0$ is a vector containing initial densities and $\hat{A}$ refers to the matrix containing generalized transmutation and decay constants.

$$\vec{N}(t) = \hat{A} \cdot \vec{N}_0 \tag{2}$$

From a practical point of view, the MCB combines the MCNP [2] and TTA [4] codes. The MCNP code is a general-purpose, continuous-energy, time-dependent, generalized-geometry coupled neutron/photon/electron transport code. The transmutation trajectory analysis code (TTA) calculates density evolutions and formation of new isotopes using the linear chain method to solve Bateman equations. In order to perform reliable calculations, the user needs to specify physical parameters, which describe in a straightforward manner the transmutation system being considered. The numerical parameters may be categorized in a number of ways: material specification and material processing, time specification, control parameters and auxiliary parameters. At the beginning of every time step, the MCB calculates neutron flux in all cells filled with burnable materials. The calculated flux is constant during the irradiation step. The new nuclides densities are estimated at the end of the time step according to the TTA method, and so on until all burn-up steps are completed. The final results are printed out in a small number of output files containing different parameters, which facilitates further data processing and elaboration.

Nuclear data libraries

The reliable results of numerical modelling not only depend on the advanced numerical method but also on linked nuclear data libraries. For that reason, the MCB code can utilize any continuous cross section data libraries. The code was successfully tested with JEF2.2, JEFF3.1, JENDL [17], ENDF/B [10] nuclear data cross section files. The nuclear data concerning the formation of new nuclides and radioactive nuclide properties are described in four additional burn-up libraries distributed with the MCB package. The libraries incorporate: the decay scheme for about 2400 isotopes based on the Table of Isotopes 8E [8] and dose data of 738 nuclides according to Council Directive 96/29/EURATOM; isomer formation ratios due to reaction (n,2n), decay and neutron capture from ORIGEN code [5]; neutron energy-dependent formations ratio of ^{242m}Am and ^{244m}Am based on Mann and Schenter's model [16]; and fission product yield for 36 heavy nuclides based on the Wahl model [18].

Two sets of nuclear data libraries were used in order to investigate sensitivity to the different cross section evaluations on fission power and actinide concentrations. The final version of the older Joint Evaluated File libraries (JEF2.2) was produced in 1993. The main scope of the JEF project was to improve the performance of existing reactors and the fuel cycle. Version 3.1 of the more recent Joint Evaluated Fission and Fusion (JEFF) cross section libraries was published in May 2005. The aim of the JEFF3.1 evaluation was to produce universal nuclear data libraries, which could be applied in many industrial applications such as: medical applications, nuclear fusion, GEN IV reactors, etc.

Results

Fuel depletion

The fuel depletion analysis focuses on the evolution of the total actinide concentration, lumped Am, lumped Pu, ^{241}Am, ^{242m}Am, ^{242}Cm, ^{239}Pu and ^{4}He. In the samples containing an initial Pu fraction, we also find a concentration of ^{241}Pu, which makes a significant contribution to fission power. In case of Pu, we mainly based our analysis on the cumulative Pu concentrations, without subdivision to particular isotopes. However, we show final concentration of ^{239}Pu and ^{241}Pu, as above mentioned.

The depletion calculations were performed as a series of independent MCB runs. Each run corresponds to the single irradiation cycle and was characterized by the different neutron spectrum and external source strength obtained in the MOTIF calculations. The high precision calculations using 10^7 neutron histories in every time step ensure that the level of relative error for all relevant flux based tallies is substantially below 0.5%. Figure 4 displays neutron spectrum in all five irradiated samples at the end of life (EOL) and Fig. 5 presents example comparison of isotope mass time-evolutions for sample 3. The right-hand side plots the mass evolution and on the left-hand side the percentage differences between libraries, expressed as the JEFF3.1 mass minus the JEF2.2 mass divided by the JEFF3.1 mass (Δ%). The difference Δ expresses the cumulative change in isotopic concentrations due to usage of different transport cross section sets (JEF2.2 and JEFF3.1). The exact differences at EOL are set out in Table 3 and the to-

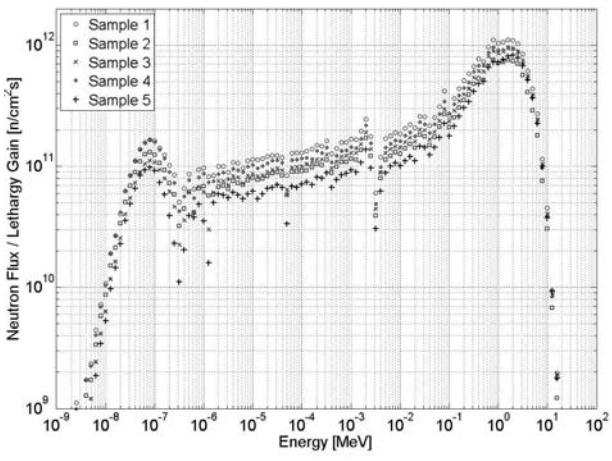

Fig. 4. Neutron flux at EOL (240.7 days).

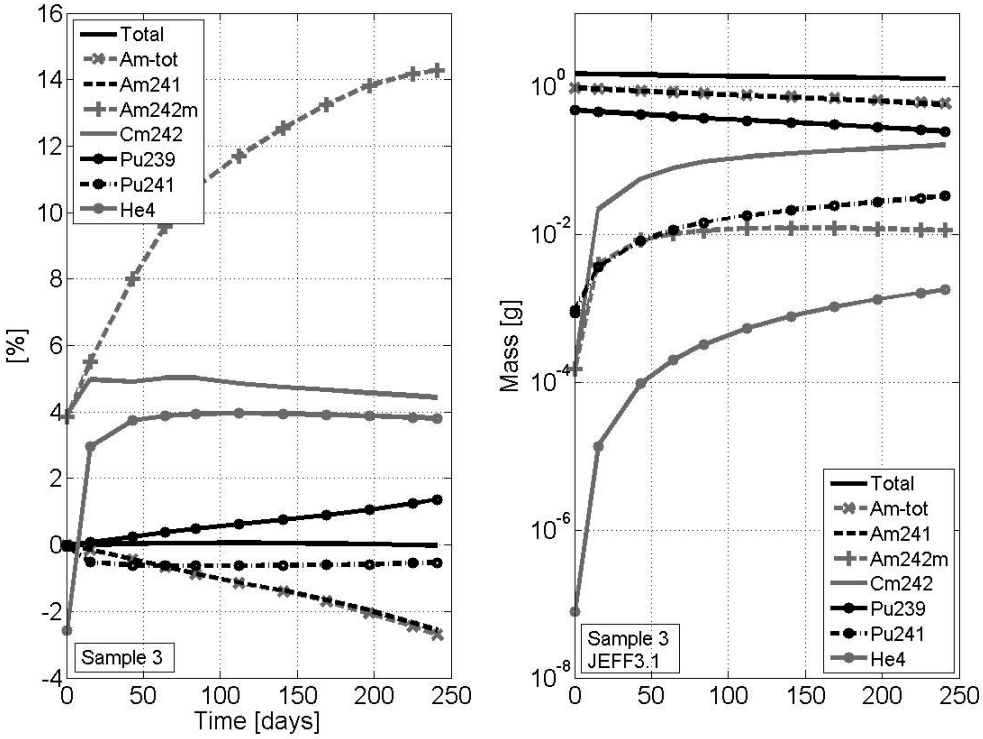

Fig. 5. Comparison of isotope masses using JEF2.2 and JEFF3.1 libraries for sample 3.

Table 3. Final concentrations and relative differences between JEF2.2 and JEFF3.1 libraries for chosen isotopes at EOL

Isotope	S1		S2		S3		S4		S5	
	JEFF3.1 (g)	Δ (%)	JEFF3.1 (g)	Δ (%)	JEFF3.1 (g)	Δ (%)	JEFF3.1 (g)	Δ (%)	JEFF3.1 (g)	Δ (%)
^{239}Pu	1.35E–02	4.73	8.63E–03	4.18	2.50E–01	1.36	1.34E–02	4.59	8.98E–01	0.28
^{241}Pu					3.32E–02	–0.53			6.60E–02	–0.56
^{241}Am	3.82E–01	–4.85	4.90E–01	–3.09	5.74E–01	–2.57	4.21E–01	–4.34	2.59E–01	–2.66
^{242m}Am	8.22E–03	14.26	9.54E–03	14.68	1.14E–02	14.27	8.57E–03	14.46	5.17E–03	14.45
^{242}Cm	2.19E–01	4.61	1.75E–01	4.41	1.64E–01	4.43	2.22E–01	4.45	6.57E–02	5.01
^{4}He	2.57E–03	4.24	1.99E–03	3.81	1.82E–03	3.81	2.57E–03	3.96	7.15E–04	4.32

$\Delta = (m_{JEFF3.1} - m_{JEF2.2})/m_{JEFF3.3}$.

tal depletion rates in the FIMA units are shown in Table 4. We present them as a percentage of initial actinide mass, which undergoes fission or decay. The depletion of lumped Am and Pu also involves transmutation to the other actinides.

Americium

The depletion of lumped Am is highest in samples 1 and 4, which corresponds to the highest source strengths for these samples. The JEFF3.1 libraries show an Am depletion rate which is about 1.5–2.5% higher than the JEF2.2 libraries for all five samples. The negative difference in ^{241}Am between JEFF3.1 and JEF2.2 increases in time and reaches the maximum value for sample 1, namely 4.85%. The lumped Am consists mainly of ^{241}Am, which means that the curves representing both ^{241}Am and lumped Am depletion are almost superimposed. The difference in ^{242m}Am is considerable and equals about 14.5% for all samples. It points to a significant change in the neutron capture cross section on ^{241}Am comparing JEF2.2 and JEFF3.1.

Plutonium

The depletion of lumped Pu is presented only for the samples with the initial Pu component. The depletion of Pu is the same for JEFF3.1 and JEF2.2 libraries for

Table 4. Depletion of lumped actinides, Am and Pu

Sample	JEF2.2			JEFF3.1		
	FIMA (%)	Am (%)	Pu (%)	FIMA (%)	Am (%)	Pu (%)
S1	7.26	53.30		7.73	55.80	
S2	5.15	42.07		5.45	44.00	
S3	14.49	36.52	4.99	14.49	38.19	3.26
S4	6.88	51.38		7.32	53.73	
S5	23.13	33.12	24.20	23.11	34.86	24.20

sample 5, whereas calculations using JEF2.2 libraries in sample 3 show a higher depletion rate. The initial fractions of Pu and Am play leading role in this case. The effect of Pu accumulation due to the transmutation from the initial Am fraction is lower in sample 5 than in sample 3. Consequently, the depletion rate is higher in sample 5 and lower in sample 3. The positive difference in ^{239}Pu concentration for samples 3 and 5 increases cycle by cycle, whereas in the remaining three samples it seems to increase just at the beginning of irradiation and then attains quite a stable value. The maximum difference at EOL also depends on the initial Pu fraction. In samples 3 and 5 the Pu produced due to the transmutation represents only a minor part of the whole Pu concentration, which means that the differences between libraries are smaller. On the other hand, in samples 1, 2 and 4 whole Pu is produced due to transmutation from the initial Am fraction; therefore its final concentration is much more sensitive to the cross section evaluations.

Curium

The curium inventory consists mainly of ^{242}Cm. It increases in concentration during the irradiation time for all five samples. The main transmutation following its formation is β decay of ^{242}Am. The sensitivity analysis to JEF2.2 and JEFF3.1 libraries shows that the differences increase at the beginning of life (BOL) and then decrease during the irradiation time. At the EOL they range from 4.4 to 5%, depending on the sample. Samples 1 and 4 show the highest final concentrations of ^{242}Cm, due to both the comparable initial concentration of Am and the source strengths. The lowest value was observed in sample 5, where the initial Am concentration was also the lowest.

Helium

The positive differences in ^{4}He concentrations range from about 3.8 to 4.3% for all irradiated samples. Its maximum accumulation can be observed in samples 1 and 4, with the minimum accumulation in sample 5. The main source of He is α decay of curium isotopes, especially ^{242}Cm, formed as a result of the neutron capture on americium isotopes. Therefore, the concentration of ^{242}Cm determines the He production. As a result, the highest concentration of ^{242}Cm in samples 1 and 4 corresponds to the highest He production, whilst the lowest concentration in sample 5 corresponds to the lowest He production.

Fission power

The MCB calculates fission power using Q_{fission} values incorporated in standard cross section libraries. The Q_{fission} includes kinetic energy of fission fragments, neutrons and prompt gammas released in the fission process of the particular actinide. Thus, Q_{fission} corresponds to the total prompt energy liberated per fission event. The energy released due to the radioactive decay of short-lived fission products and other long-lived nuclides is automatically added to the fission power P_q in the MCB code.

Figure 6 presents fission power time-evolution for samples without the initial Pu fraction, whereas Fig. 7 is shown with the initial Pu fraction. The sensitivity of P_q to the different cross section evaluations was checked by performing two sets of calculations making use of the JEFF3.1 and the JEF2.2 nuclear cross section libraries. The P_q was calculated exactly in the middle of all nine irradiation cycles (C1–C9). Three additional points were added to investigate the fission power at the BOL, after 12 h of irradiation and at EOL.

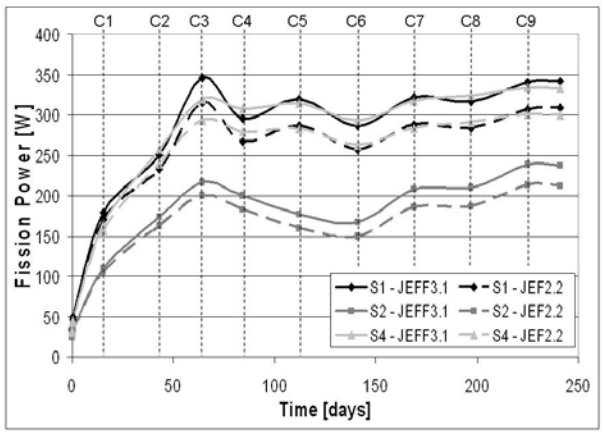

Fig. 6. Power evolutions for samples 1, 2 and 4.

The power profiles during 240 days of irradiation for samples 1, 2 and 4 show a similar trend. The increase in fission power from the BOL due to the formation of fissile nuclides started from the transmutation of ^{241}Am. In the first stage of irradiation, fission power is driven by the fission of americium isotopes. ^{242m}Am bred by the neutron capture from ^{241}Am plays the leading role. The fission cross section of ^{242m}Am is of the order of magnitude of a few thousand barns in the thermal neutron spectrum. In the later stages, fission of other actinides, especially ^{239}Pu, makes a significant contribution to the released power. The absolute value of the P_q corresponds mainly to the source strengths obtained in previous transport calculations (Table 2). The source strengths for samples 1 and 4 differ only by about 12%, whilst for sample 2 the difference is much greater. The reason for this is the axial placement of the samples in the experiment (Fig. 1). Despite the fact that samples 1 and 4 are placed in different specimen holders (HELIOS-1 and HELIOS-2), their axial position in the HFR core is the same. Therefore, the effect of flux buckling has a comparable influence on both samples mentioned. In addition, the four slight peaks for cycles 3, 5, 7 and 9, observed in sample 1, refer to the change in orientation of the HELIOS experiment

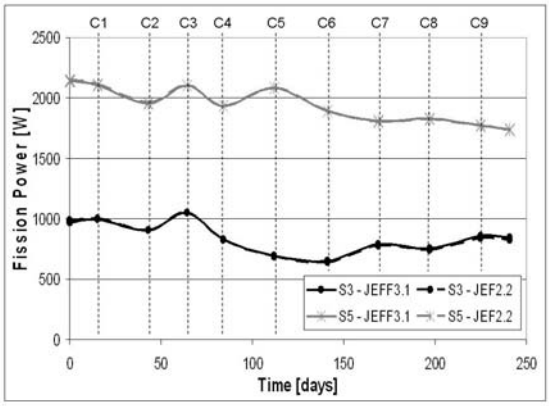

Fig. 7. Power evolutions for samples 3 and 5.

by 180°. For other cycles and samples this effect is less visible. In general, the influence of the rotation is more significant for the HELIOS-1 (samples 1 and 3) than for the HELIOS-2 (samples 2, 4 and 5), which could also be seen in Table 2. The reason for that is the decrease in neutron flux due to the presence of CR in the in-core position F6. After rotation, HELIOS-1 is closer to CR than HELIOS-2. The sensitivity studies to the cross section libraries show that P_q calculated using JEFF3.1 libraries is higher than the results obtained using JEF2.2 libraries. This effect is explained by the higher production and subsequent incineration of metastable ^{242m}Am for JEFF3.1 calculations.

The trends for samples 3 and 5 show different power profiles from those of the other three samples. The cross section sets applied do not influence the power profiles and the presented curves are superimposed. The fission power in sample 5 is much higher than for sample 3 because of the higher initial fraction of Pu isotopes. The decrease in power for this sample is simply caused by Pu incineration. The smooth part of the fission power profile between the third and sixth irradiation cycle for sample 3 is similar to the profile for sample 2, but the absolute power values are much higher. This can be explained by the similar irradiation environment for both samples. They are placed in different specimen holders, but at the same vertical level, at the top of the experiment. The lowest CR and the highest VDU position caused the diminution of flux and, as a result, a loss of peak power in the fifth irradiation cycle for these two samples. The fission power released in sample 3 corresponds mostly to fissioning of ^{239}Pu, ^{242m}Am and ^{241}Pu and in sample 5 to fissioning of ^{239}Pu, ^{241}Pu and ^{242m}Am, respectively.

Conclusions

The new method of numerical analysis of irradiation experiments in the HFR Petten was developed at the Joint Research Centre – JRC, Institute for Energy – IE (The Netherlands) in collaboration with the AGH University (Krakow, Poland). The IE was main developer of the method presented and AGH provided the numerical tools. The method was originally applied to depletion analysis of the HELIOS experiment.

The sensitivity of results to JEFF3.1 and JEF2.2 cross section libraries show significant differences in the rate of accumulation of ^{242m}Am. The results obtained in the JEFF3.1 calculations show values about 14.5% higher than for JEF2.2, which is extremely significant in terms of predicting the power released, not only in the HELIOS samples but also in all reactor systems dedicated to incineration of MA fuels. The differences in concentrations between other investigated isotopes are below 5% in absolute value. The final Am incineration is in line with source strengths obtained in previous transport calculations.

The future analysis of the HELIOS experiment will focus on comparative studies between numerical results and experimental measurements. There are plans for experimental post irradiation examination of the HELIOS samples in the framework of the European Commission's FAIRFUELS project [11].

Acknowledgment. The authors appreciate the support of all the institutions involved in IP EUROTRANS and also the financial support of the European Commission in frame of a contract FI6W-CT-200-516520.

References

1. Blachot J, Assal W, Blaise P *et al*. (2000) The JEF2.2 Nuclear Data Library. JEFF Report no. 17. NEA OECD
2. Booth TE, Brown FB, Bull JS *et al*. (2005) X-5 Monte Carlo Team: MCNP-A General Monte Carlo N-Particle Transport Code. Version 5. LANL Report LA-UR-03-1987
3. Cetnar J (2006) General solution of Bateman equations for nuclear transmutations. Ann Nucl Energ 33:640–645
4. Cetnar J, Gudowski W, Wallenius J (1999) MCB: A continuous energy Monte Carlo burn-up simulation code. In: Proc of Actinide and Fission Product Partitioning and Transmutation. EUR 18898 EN, OECD/NEA 523
5. Croff AG (1980) A User's manual for the ORIGEN2 computer code. ORNL/TM-7157
6. D'Agata E (2009) HELIOS, Irradiation of U-free fuels and targets for Am transmutation in a QUATRO rig with two sample holders at the HFR Petten. Project no. 325 002. Design and Safety Report, PUBSY no. JRC46049
7. Döderlein C (2010) User guide for the improved neutronics schema for the interpretation of irradiation experiments in the HFR. Part 1: Calculation of the environment. European Commission, Directorate-General Joint Research Centre, Institute for Energy – Safety of Future Nuclear Reactors Unit, PUBSY no. JRC59903
8. Firestone RB, Shirley VS (1996) Table of isotopes 8E. Wiley
9. Forrest RA (2003) FISPACT-2003 User manual. EASY Documentation Series, UKAEA FUS 485
10. Herman M, Trkov A (2009) ENDF-6 Formats Manual, Data Formats and Procedures for the Evaluated Nuclear Data File ENDF/B-VI and ENDF/B-VII, CSEWG Document ENDF-102. Report BNL-90365-2009
11. Klaassen FC (2009) Project presentation, project's full name FAIRFUELS. Contract (grant agreement) no. 232624, www.fp7-fairfuels.eu
12. Klaassen FC, Schram RPC, Bakker K *et al*. (2002) Spinel inert matrix fuel testing at the HFR Petten. In: Proc of the 7th Information Exchange Meeting on Actinide and Fission Product Partitioning and Transmutation, Jeju, Republic of Korea
13. Koning A, Forrest R, Kellet M *et al*. (2006) The JEFF-3.1 Nuclear Data Library. JEFF Report no. 21. NEA OECD
14. Konings RJM, Conrad R, Dassel G *et al*. (2000) The EFTTRA-T4 experiment on americium transmutation. Jur Nucl Mat 282:159–170
15. Konings RJM, Mühling G, Conrad R *et al*. (1998) Transmutation of americium and technetium: Recent results of EFTTRA. In: Proc of 5th OECD/NEA Information Exchange Meeting on Actinide and Fission Product Partitioning and Transmutation. SCK-CEN, Mol, Belgium
16. Mann FM, Schenter RE (1977) Calculated neutron capture cross-section to the americium ground and isomer states. Nucl Sci Eng 63:242–249
17. Shibata K, Iwamoto O, Nakagawa T *et al*. (2011) JENDL-4.0: A new library for nuclear science and engineering. J Nucl Sci Technol 48;1:1–30
18. Wahl A (1985) Nuclear-charge distribution near symmetry for thermal-neutron-induced fission of ^{235}U. Phys Rev C 32:184–194